A Nanozyme-linked immunosorbent assay for Aflatoxin B1 detection with High Sensitivity and Excellent Reproducibility

Shuang Peng
Changsha University of Science & Technology
Kai Li
Changsha University of Science & Technology
Yi-xuan Wang
Changsha University of Science & Technology
Lin Li
Changsha University of Science & Technology
Yun-Hui Cheng
Changsha University of Science & Technology
Zhou Xu (xz_jnu@126.com)
Changsha University of Science & Technology

Research Article

Keywords: Immunoassay, Metal-organic framework, Nanozyme, Aflatoxin B1, Dispersion, Reproducibility

Posted Date: May 18th, 2022

DOI: https://doi.org/10.21203/rs.3.rs-1641617/v1

Abstract

The nanozyme-linked immunosorbent assay (NLISA) has attracted increasing attention for detecting mycotoxin due to its excellent specificity and low-cost. However, the dispersion of most nanozymes is not desirable, which usually leads to poor reproducibility of detection. Herein, we generated a novel porous Iron-Porphyrin-Zr-MOF NanoPCN-223(Fe) with outstanding dispersion and superior peroxidase-like activity. The excellent dispersion and catalytic performance of NanoPCN-223(Fe) was exploited to establish an enhanced dispersion MOF-linked immunosorbent assay (Ed-MOFLISA) to detect aflatoxin B1 in real food samples. The optimized Ed-MOFLISA displayed a broad quantitative range from 0.05 to 10 ng/mL and a limit of detection of 0.003 ng/mL. The recovery of spiked peanut milk and soy milk ranged from 91.22–97.63%. Intra-assay and inter-assay coefficient of variation values ranged from 0.78 to 3.85%, demonstrating the outstanding reproducibility and accuracy of Ed-MOFLISA. The findings indicate the suitability of novel NanoPCN-223(Fe) with enhanced dispersion for NLISA in food safety analyses.

1. Introduction

Food safety is paramount to all of us. Aflatoxin B1 (AFB1) is a secondary metabolite produced by *Aspergillus flavus*(Wang et al. 2021). The fungal mycotoxin is the most toxic mycotoxin known, with mutagenic(Zavala-Franco et al. 2020), teratogenic(Oliveira et al. 2021), immunosuppressive(Myndrul et al. 2021) and carcinogenic effects(Azaiez et al. 2014; Rushing and Selim 2019). AFB1 is classified as a Group I carcinogen by the International Agency for Research on Cancer(He et al. 2019). Low-cost, stable, and large-scale technology that directly detects AFB1 in food samples is needed to realize real-time monitoring and control of AFB1 contamination of food. Current methods to detect AFB1 include liquid chromatography-tandem mass spectrometry (LC-MS/MS), high-performance liquid chromatography, and enzyme-linked immunosorbent assays (ELISA) (Zhang et al 2018). The latter is the most commonly used detection method for AFB1 because of its convenience and highly sensitive detection capability(Lei et al. 2020; You et al. 2021). The enzymatic process of ELISA permits signal amplification(Jiang et al. 2020). Natural enzymes have high catalytic efficiency(Shen et al. 2022) and specificity under physiological conditions(Li and Head-Gordon 2021). However, disadvantages that include high production and purification costs and variability limit their applications.

Nanozymes are nanomaterials with intrinsic enzyme-like characteristics. Nanozymes that include metals(Yu et al. 2019), metal compounds(Lin et al. 2021), and metal-organic framework (MOF)(Shen et al. 2022) have better stability and lower cost than natural enzymes. In addition, other unique properties of nanomaterials can endow nanozymes with more functions(Xu et al. 2020). Therefore, The nanozyme linked immunosorbent assay (NLISA) has attracted increasing attention for analytical detection due to its excellent specificity and low-cost. Among the various types of nanozymes, porous materials like MOFs possess many active sites, and high specific surface areas(Gorle et al. 2021; Li et al. 2021), and have excellent potential for catalysis(Huang et al. 2021). Therefore, MOFs can serve as an ideal nanozyme to improve the detection stability of NLISA(Wang et al. 2022). Recently, our group used the MIL-88 MOF to replace natural enzymes, such as horseradish peroxidase (HRP), to create an MOF-linked immunosorbent

assay (MOFLISA)(Xu et al. 2021a). However, most MOF crystals have a strong tendency to aggregate in solution. Their poor dispersion(Lee et al. 2019; Xu et al. 2021b) hampers their detection reproducibility(Zhao et al. 2015). Therefore, a strategy to improve the sensitivity and stability of NLISA for direct detection of AFB1 in foods is imperative.

Inspired by previous work, we found that acid modulators can alter the surface potential of MOFs with carboxyl ligands(Jiang et al. 2019), which enhances dispersion(Prabhu et al. 2019). Herein, we describe a strategy that uses acetic acid modulation. The inhibited deprotonation of iron-porphyrin linkers increases the surface potential, thereby enhancing the dispersion of the traditional PCN-223(Fe). The novel NanoPCN-223(Fe) has excellent peroxidase activity and colloidal stability. An enhanced dispersion MOFFLISA (Ed-MOFLISA) based on NanoPCN-223(Fe) nanozyme catalysis was successfully achieved to improve the detection reproducibility of AFB1. The findings indicate the suitability of the novel NanoPCN-223(Fe) nanozyme in food safety control.

2. Materials And Methods

2.1 Reagents and chemicals

The standards of AFB1, aflatoxin B2 (AFB2), aflatoxin G1 (AFG1), aflatoxin G2 (AFG2), zearalenone (ZEA) and ochratoxin A (OTA) were purchased from Dr. Ehrenstorfer (Augsburg, Germany). AFB1-specific antibody and antigen were acquired from Lvkang company (Wuxi, China). 1-Ethyl-3-[3-dimethylaminopropyl] carbodiimide hydrochloride (EDC), N-hydroxy succinimide (NHS), terephthalic acid (TA) and acetic acid were purchased from Sigma–Aldrich (St Louis, MO, USA), $ZrOCl_2 \cdot 8H_2O$, triethylamine (TEA), 3,3’,5,5’-Tetramethylbenzidine (TMB), H_2SO_4 (98%), KBr, H_2O_2, N 'N-Dimethylformamide (DMF) and 5,5-dimethyl-1-pyrroline N-oxide (DMPO) were purchased from Sinopharm Chemical Reagent Company (Beijing, China). Millipore Milli-Q ultrapure (18.2 MΩ; MerckMillipore, Darmstadt, Germany) water was used throughout the whole study. All other reagents were of analytical reagent grade. The instruments details are described in the Supplementary Material.

2.2 Instrument

Fourier-transform infrared spectroscopy (FTIR) spectra analyses was conducted on a Spectrum GX (Perkin-Elmer, United States). The crystal phase was investigated using a BRUKER AXS D8-Advance X-ray diffraction (XRD) system (Bruker Corp, Billerica, MA, USA). Transmission electron microscopy (TEM) images were obtained with a TecnaiG2 F20 (FEI Co. Hillsboro, OR, USA) operated at an accelerating voltage of 200 kV. The size and zeta-potentials of the formed nanomaterial were measured using a dynamic laser light scattering instrument (DLS) using a Zeta sizer nano ZS (Malvern Instruments, Malvern, UK). Ultraviolet–visible (UV–vis) absorption spectra were recorded on a UV-2550 Spectrophotometer (Shimadzu Corporation, Kyoto, Japan).

2.3 Synthesis of traditional PCN-223(Fe)and NanoPCN-223(Fe)

Traditional PCN-223(Fe) was fabricated as previously described(Zhang et al. 2020). NanoPCN-223(Fe) was fabricated as previously described with some modifications(Zhang et al. 2020). Briefly, 4.056 mg Fe (III) tetra(4-carboxylphenyl) porphyrin chloride (Fe III–TCPPCl) and 18 mg $ZrOCl_2$•$8H_2O$ were added to 14.4 mL dimethylformamide (DMF) and stirred for 30 min. Triethanolamine (TEA, 16 μL) and 3.6 mL acetic acid were added and the complete solution was stirred for 10 min and then placed in a reaction kettle. The kettle was heated in an oven at 65°C for 5 days. After cooling to room temperature, the obtained products were collected by centrifugation at 625 g for 10 min, washed with DMF three times, and oven-dried. TEA and acetic acid effectively controlled the crystal size of the material.

2.4 Peroxidase-like activity assay and kinetic analysis of NanoPCN-223(Fe)

Peroxidase-like activity of NanoPCN-223(Fe) was determined using a typical substrate, 3,3´,5,5´-tetramethylbenzidine (TMB) or hydrogen peroxide (H_2O_2). The blue-coloured oxidized TMB (oxTMB) was detected by ultraviolet-visible (UV–vis) spectrometry; the adsorption peak was 652 nm. The experiments were performed by maintaining one substrate concentration constant while adjusting the concentration of the other substrate. The experiments were performed at 45°C in acetic acid-sodium acetate (NaAc-Hac) buffer (2 M, pH 4.5) with a final nanozyme concentration of 0.01 mg/mL. When changing the TMB concentration, the concentration of the H_2O_2 substrate was fixed at 0.3 mM. When H_2O_2 was used as the substrate, the TMB concentration was fixed at 1.0 mM. The absorbance at 652 nm was measured. The Michaelis–Menten constant (K_m) and maximum initial velocity (V_{max}) were calculated according to the Michaelis–Menten equation (Xu et al. 2021b):

$$\nu = \frac{\nu_{\max}[S]}{K_m + [S]}$$

where v represents the initial reaction rate, K_m represents the Michaelis constant, v_{max} represents the maximal reaction rate, and [S] represents the substrate concentration.

2.5 Conjugation of MOF and antibody 2

Secondary antibodies were immobilised on the MOF surface of by covalent coupling(Fu et al. 2018; Ma et al. 2016). Briefly, amino-functionalized MOFs (1 mg/mL) was mixed with 7.5 mg 1-ethyl-3-(3-dimethylaminopropyl)carbodiimide (EDC) and 3 mg N-hydroxysuccinimide (NHS) and stirred for 15 min. The mixture was centrifuged at 3000 rpm for 10 min to remove unreacted NHS and EDC. Finally, antibody 2 (Ab_2, 2 mg/mL) was added dropwise to the MOF solution under magnetic stirring at 37°C. The sample was stirred for 8 h and the obtained functional MOF was dispersed in phosphate-buffered saline (PBS) and stored at 4°C until use.

2.6 Construction of Ed-MOFLISA

Scheme 1 depicts the creation of this AFB_1 detection biosensor. 100 μL AFB_1 antigen was added to each well of a multi-well plate and incubated at 37°C for 2 h. Each well was washed three time with PBS

containing Tween (PBST) then blocked with 1% bovine serum albumin in PBS and incubated at 37°C for 2 h. The wells were washed three times with PBST. Each well then received 50 µL of the antibody suspension and different concentrations of AFB_1, followed by incubation at 37°C for 30 min. After washing three times with PBST, 16 µL MOF@Ab_2 suspension was added to each well, followed by incubation at 37°C for 30 min. The wells were washed three times with PBST and 188 µL of HAC-NaAC buffer (0.2 M, pH = 4), 1 µL of H_2O_2 solution (25 mM, final concentration of 10 µM), and 10 µL of TMB solution (25 mM, final concentration of 1 mM) were added to each well. The plate was incubated at 45°C for 20 min. The UV spectra and absorbance were recorded at 450 nm after the reaction was terminated by the addition of adding 50 µL of 0.2 M H_2SO_4.

2.7 Specificity analysis

To study the specificity, the interference of various AFB_1 analogues, including AFB_2, AFG_1, and AFG_2, and other mycotoxins, including zearalenone (ZEA) and ochratoxin A (OTA) was studied. AFB_1 (5 ng/mL) or 25 ng/mL of AFB_2, AFG_1, AFG_2, ZEA, or OTA were individually added to the sensing system and analyzed as described above.

2.8 Detection of AFB1 in grain drink samples

To verify the feasibility and accuracy of Ed-MOFLISA in actual samples, peanut milk and soy milk purchased from local supermarkets were used for testing. Blank grain drink was spiked with different concentrations of AFB1 (0.01, 0.1, 1 ng/mL) and then extracted with methanol–water (30 mL, 8:2 v/v) under gentle stirring on a shaker for 5 min. The samples were centrifuged at 5000 g for 10 min to remove the fat layer. The supernatant was filtered through a 0.22 µm syringe filter to remove impurities. The obtained aqueous phase was analyzed.

3. Results And Discussion

3.1 Characterization of NanoPCN-223(Fe)

In order to characterize the successful synthesis of NanoPCN-223(Fe), Fourier-transform infrared spectroscopy (FTIR) and X-ray diffraction (XRD) analyses were performed. Characteristic FTIR absorption peaks absorption was evident at 1009 cm^1 (Fig. 1a). These could be ascribed to the porphyrin ring from iron-porphyrin linkers(Fularz et al. 2021). Vibration peaks evident at approximately around 650 cm^1 of Zr-O bond from porphyrin-Zr MOF indicated the successful coordination of metal salts and ligands. In addition, the XRD pattern (Fig. 1b) showed that the structure of the NanoPCN-223(Fe) was consistent with the traditional PCN-223(Fe) and simulated structures. The FTIR and XRD findings clearly demonstrated the successful synthesis of NanoPCN-223(Fe). Traditional PCN-223(Fe) displayed a spindle shape with wide size distribution (Fig. 1c **and d**). However, NanoPCN-223(Fe) displayed a short rod-like shape and uniform size. And the insert exhibit that NanoPCN-223(Fe) owns better dispersion in an aqueous solution. These results indicated the enhanced dispersion and uniformity of NanoPCN-223(Fe) compared with traditional PCN-223(Fe).

Insert Fig. 1

3.2 Dispersion of NanoPCN-223(Fe) and MIL-88

To further confirm the enhanced dispersion of NanoPCN-223(Fe) compared with traditional PCN-223(Fe) and MIL-88, the hydrodynamic diameter and zeta-potential of these three kinds of nanoparticles on a dynamic light scattering (DLS) instrument with a scattering angle of 90°at 37°C was tested. The polydispersity index (PDI) is frequently used as an indicator for dispersion of particles in suspensions(Zaib et al. 2020). Lower PDI values indicate better dispersion of particles, with a limit of 0.1(Baalousha and Lead 2012). As shown in Fig. 2a-c, DLS of NanoPCN-223(Fe) revealed a narrower size distribution with a lower PDI (0.107 ± 0.067) compared to traditional PCN-223(Fe) (0.386 ± 0.038) and MIL-88 (0.357 ± 0.036). The findings indicate the pronounced dispersion of NanoPCN-223(Fe) nanoparticles. The NanoPCN-223 surface had higher positive charges (+ 20.16 ± 0.39 mV) than traditional PCN-223(Fe) (+ 5.08 ± 0.26 mV) and MIL-88 (-7.18 ± 0.32 mV) (Fig. 2d). This may reflect the inhibited deprotonation of carboxyl linkers(Jiang et al. 2019), resulting in enhanced dispersion of NanoPCN-223(Fe).

Insert Fig. 2

3.3 Kinetic assays of NanoPCN-223(Fe)

To investigate the peroxidase-like activity of NanoPCN-223(Fe), the oxidation reaction kinetic for TMB was studied. Figure 3 shows typical Michaelis–Menten curves and double-reciprocal plots. The findings indicate that the reaction catalyzed by NanoPCN-223(Fe) followed Michaelis–Menten kinetics. To clearly and conveniently express the experimental results, the K_m and V_{max} values for TMB and H_2O_2 were compared with other catalysts. The findings are summarized in **Table S1**. The K_m value of NanoPCN-223(Fe) for H_2O_2 of 2.0×10^{-4} M was approximately 19- and 85-fold lower than that of HRP(Aghayan et al. 2019) and MIL-88(Xu et al. 2021a), respectively. Moreover, the obtained V_{max} of NanoPCN-223(Fe) was higher than that of HRP(Aghayan et al. 2019) and MIL-88(Xu et al. 2021a), indicating that NanoPCN-223(Fe) has superior peroxidase-like activity and higher affinity than HRP and MIL-88 toward the H_2O_2 substrate during the catalytic process. The high catalytic activity of iron-porphyrin and the robust structures of MOFs can make each iron-porphyrin accessible by substrates, and prevent the self-dimerization of reaction centers(Ling et al. 2016). These results clearly demonstrate that the NanoPCN-223(Fe) could significantly enhance dispersion due to the superior peroxidase-like activity and high affinity.

Insert Fig. 3

3.4 NanoPCN-223(Fe)-based Ed-MOFLISA for detection of AFB1

The capability of NanoPCN-223(Fe) to improve the performance of Ed-MOFLISA was further tested by coupling NanoPCN-223(Fe) with antibody 2 (Ab_2). DLS confirmed the successful construction of the

NanoPCN-223(Fe)@Ab_2. NanoPCN-223(Fe) was observed with an average size and zeta-potential of 205.46 nm and + 20.16 mV, respectively (Fig. 2b, d). After adding the antibody, the particle size increased to 237.81 nm (Fig. 4b) and the zeta-potential became − 3.54 mV (**Fig. S1a**). These findings proved that NanoPCN-223(Fe) and Ab_2 successfully coupled. The peroxidase activity of NanoPCN-223(Fe)@Ab_2 was still close to that of bare NanoPCN-223(Fe) (**Fig. S1b**), indicating that the conjunction did not affect the catalytic activity of NanoPCN-223(Fe). MOFLISA based on NanoPCN-223(Fe) nanozyme catalysis was successful, as shown in Scheme 1. In this method, the NanoPCN-223(Fe) catalyzes oxidation of colorless TMB to blue oxTMB via the formation of ·OH radicals in the presence of H_2O_2(Huo et al. 2019). As a proof-of concept, in the presence of AFB1, less NanoPCN-223(Fe)@Ab_2 conjugates remained in the assay wells, resulting in a lighter color. To improve the sensitivity of AFB_1 detection, we optimized the key parameters. Antigen at a concentration of 2 μg/mL, antibody at 3 μg/mL, NanoPCN-223(Fe)@Ab_2 at 0.6 μg/mL, and a 1:200 coupling ratio of NanoPCN-223(Fe) to secondary antibody produced the highest absorbance (**Fig. S2 a–d**). Under the optimized conditions, the detection limit of AFB_1 was 0.003 ng/mL (S/N = 3) with a 3.3 s/slope (s, standard deviation of the blank samples) and wide linear range (0.005 to 10 ng/mL) (Fig. 4c **and d**). Compared with the other immunoassays shown in **Table S2**, the Ed-MOFLISA displayed a wider linear relationship, indicating a better response to high concentrations of AFB_1. Moreover, the limit of detection of Ed-MOFLISA was approximately 3-fold lower than that of MOFLISA based on MIL-88 (0.009 ng mL^{-1}), suggesting more sensitivity to AFB_1. The collective findings indicate the potential of NanoPCN-223(Fe)-based Ed-MOFLISA in detecting AFB_1 and other concerning small bio-molecules.

Insert Fig. 4

3.5 Real sample analysis

Specificity is essential to ensure Ed-MOFLISA is a general and reliable method for the AFB1 detection in complex foods. To investigate the specificity of Ed-MOFLISA, several AFB_1 analogues, including AFB_2, AFG_1, and AFG_2, and mycotoxins ZEA and OTA (25 ng/mL), were investigated with a concentration that was 5-times higher than the AFB_1 (5 ng/mL). As shown in Fig. 4e, only AFB_1 resulted in a significant signal change. The effects of the other aflatoxins were negligible. These results indicated that the Ed-MOFLISA has a specific recognition and excellent selectivity for detecting AFB1.

Ed-MOFLISA appeared to be acceptable for detecting AFB_1 in real samples. The following experiments were performed to confirm the application of Ed-MOFLISA in actual samples. Peanut milk and soy milk samples were purchased from local supermarkets as model samples. Milk samples spiked with three different concentrations of AFB1 (0.01, 0.1, and 1 ng/mL) were examined by Ed-MOFLISA. The average recovery of the Ed-MOFLISA and MOFLISA method was 95.27% and 91.8%, respectively (Table 1). The relative standard deviation (RSD, relative to an average recovery of 100%) of the Ed-MOFLISA method (1.40%) was lower than RSD of the MOFLISA (6.20%), indicating that greater accuracy and enhanced practicality of Ed-MOFLISA compared to MOFLISA.

Table 1
Application of Ed-MOFLISA for AFB_1 determination in peanut milk and soy milk samples

samples	Added (ng/mL)	Recovery(a) (%)	Recovery(b) (%)
peanut milk	0.01	91.30 ± 0.79	91.22 ± 0.71
	0.1	96.53 ± 3.20	95.57 ± 3.50
	1	95.03 ± 1.02	94.83 ± 0.98
soy milk	0.01	95.14 ± 1.33	95.15 ± 1.78
	0.1	97.63 ± 1.65	96.10 ± 3.70
	1	95.97 ± 0.84	95.76 ± 0.87

Insert Table 1

3.6 Reproducibility analysis

Reproducibility of Ed-MOFLISA is vital for consistent performance. The coefficient of variation (CV) was calculated according to the data in Table 1 and was calculated (%) as (standard deviation/mean) ×100. Intra-assay CV values of Ed-MOFLISA ranged from 0.87 to 3.31%. Inter-assay CV values ranged from 0.75 to 3.85% (Fig. 5). Both were much lower than most other detection methods based on nanozyme in **Table S3**, including MOFLISA (2.63–10.36%), indicating the excellent accuracy and splendid reproducibility of Ed-MOFLISA. Meanwhile, we demonstrated that the catalytic activity of NanoPCN-223 remained stable at different pH values, different temperatures, or after storage for some time (**Fig. S3 a–d**). The outstanding reproducibility may be caused by the extensive dispersion of NanoPCN-223(Fe) and confirmed that Ed-MOFLISA is reliable and excellent for accurately monitoring AFB_1.

Insert Fig. 5

4. Conclusion

NanoPCN-223(Fe) nanozyme was fabricated using an acetic acid modulated strategy. The nanozyme was used to construct the Ed-MOFLISA, which analyzed the typical food safety hazard of AFB_1 in food samples. The enhanced dispersion of NanoPCN-223(Fe) nanoparticles resulted in excellent reproducibility of Ed-MOFLISA was conferred with a splendid reproducibility (< 4% variation) and satisfactory recovery (91.22–97.63%) in detecting AFB_1 compared with other fast detection methods. The findings also detail the improved dispersion of a porous nanozyme, and is a novel approach to improve the reproducibility of a nanozyme-based immunoassay. We anticipate that this method will prove useful in detecting many other targets, such as protein, toxins, or even cells and bacteria, where reproducibility is critical.

Declarations

Funding

This work was supported by the Research Foundation of Education Bureau of Hunan Province (21B0337), the Nature Science Foundation of Hunan (2021JJ30701), Research Project of the General Administration of Customs of the People's Republic of China (2020HK183), Foundation of State Key Laboratory of Utilization of Woody Oil Resource (GZKF202111).

Conflicts of interest

There are no conflicts of interest to declare.

Availability of data and material

The data that supports the findings of this study are available in the supporting information of this article.

Code availability

Not applicable

Author's contributions

Shuang Peng: Writing - review & editing.

Kai Li: Validation, Writing - Original Draft.

Yi-xuan Wang: Validation, Formal analysis.

Lin Li: Investigation.

Yun-Hui Cheng: Project administration.

Zhou Xu: Conceptualization, Writing - review & editing, Project administration.

Ethical Approval

This article does not contain any studies with human and animal subjects.

Consent to participate

Not applicable

Consent for publication

Not applicable

References

1. Azaiez I, F Giusti, Sagratini G, Maes J, M Fernández-Franzón (2014). Multi-mycotoxins analysis in dried fruit by lc/ms/ms and a modified quechers procedure. Food Anal Methods 7: 935–945. https://dx.doi.org/10.1007/s12161-013-9785-3
2. Aghayan M, Mahmoudi A, Nazari K, Dehghanpour S, Sohrabi S, et al (2019) Fe(III) porphyrin metal-organic framework as an artificial enzyme mimics and its application in biosensing of glucose and H2O2. J Porous Mat 26: 1507–1521. https://dx.doi.org/10.1007/s10934-019-00748-4
3. Alsayyah A, ElMazoudy R, Al-Namshan M, Al-Jafary M, Alaqeel N (2019) Chronic neurodegeneration by aflatoxin B1 depends on alterations of brain enzyme activity and immunoexpression of astrocyte in male rats. Ecotoxicol Environ Saf 182: 111378. https://dx.doi.org/10.1016/j.ecoenv.2019.109407
4. Baalousha M, Lead JR (2012) Rationalizing Nanomaterial Sizes Measured by Atomic Force Microscopy, Flow Field-Flow Fractionation, and Dynamic Light Scattering: Sample Preparation, Polydispersity, and Particle Structure. Environ Sci Technol 46: 6134–6142. https://dx.doi.org/10.1021/es301167x
5. Fu K, Yan Z, Li J, Liu Y, Bo P, et al (2018) Colorimetric Immunoassay for Rapid Detection of Vibrio parahemolyticus Based on Mn2 + Mediates the Assembly of Gold Nanoparticles. J Agric Food Chem 66: 9516–9521. https://dx.doi.org/10.1021/acs.jafc.8b02494
6. Fularz A, Almohammed S, Rice JH (2021) SERS Enhancement of Porphyrin-Type Molecules on Metal-Free Cellulose-Based Substrates. ACS Sustain Chem Eng 9: 16808–16819. https://dx.doi.org/10.1021/acssuschemeng.1c06685
7. Gorle DB, Ponnada S, Kiai MS, Nair KK, Nowduri A, et al (2021) Review on recent progress in metal-organic framework-based materials for fabricating electrochemical glucose sensors. J Mater Chem B 9: 7927–7954. https://dx.doi.org/10.1039/d1tb01403j
8. Huang X, Zhang S, Tang Y, Zhang X, Bai Y, Pang H (2021) Advances in metal-organic framework-based nanozymes and their applications. Coord Chem Rev 449: 214216. https://dx.doi.org/10.1016/j.ccr.2021.214216
9. Huo M, Wang L, Wang Y, Chen Y, Shi J (2019) Nanocatalytic Tumor Therapy by Single-Atom Catalysts. ACS Nano 13: 2643–2653. https://dx.doi.org/10.1021/acsnano.9b00457
10. Jiang C, Huang Y, He T, Huang P, Lin J (2020) A dual-round signal amplification strategy for colorimetric/photoacoustic/fluorescence triple read-out detection of prostate specific antigen. Chem Commun 56: 4942–4945. https://dx.doi.org/10.1039/d0cc01086c
11. Jiang D, Zhu Y, Chen M, Huang B, Zeng G, et al (2019) Modified crystal structure and improved photocatalytic activity of MIL-53 via inorganic acid modulator. Appl Catal B 255: 117746. https://dx.doi.org/10.1016/j.apcatb.2019.117746
12. Lee H-C, Heil T, Sun J-K, Schmidt BVKJ (2019) Dispersed nano-MOFs via a stimuli-responsive biohybrid-system with enhanced photocatalytic performance. Mater Horiz 6: 802–809. https://dx.doi.org/10.1039/c8mh01342j

13. Lei X, Xu X, Liu L, Kuang H, Xu L, et al (2020) Rapid quantitative determination of fentanyl in human urine and serum using a gold-based immunochromatographic strip sensor. J Mater Chem B 8: 8573–8584. https://dx.doi.org/10.1039/d0tb01509a
14. Li P, Zheng D, Gao M, Zuo X, Sun L, et al (2021) Bimetallic MOF-Templated Fabrication of Porous Zn, N Co-doped Mo2C for an Efficient Hydrogen Evolution Reaction. ACS Appl Energy Mater 4: 8875–8882. https://dx.doi.org/10.1021/acsaem.1c01085
15. Li W-L, Head-Gordon T (2021) Catalytic Principles from Natural Enzymes and Translational Design Strategies for Synthetic Catalysts. ACS Cent Sci 7: 72–80. https://dx.doi.org/10.1021/acscentsci.0c01556
16. Lin S, Hao Z, Shen J, Chang X, Huang S, et al (2021) Enhancing the CO_2 methanation activity of Ni/CeO_2 via activation treatment-determined metal-support interaction. J Energy Chem 59: 334–342. https://dx.doi.org/10.1016/j.jechem.2020.11.011
17. Ling P, Lei J, Ju H (2016) Nanoscaled Porphyrinic Metal-Organic Frameworks for Electrochemical Detection of Telomerase Activity via Telomerase Triggered Conformation Switch. Anal Chem 88: 10680–10686. https://dx.doi.org/10.1021/acs.analchem.6b03131
18. Ma H, Li X, Yan T, Li Y, Liu H, et al (2016) Sensitive Insulin Detection Based on Electrogenerated Chemiluminescence Resonance Energy Transfer between Ru(bpy)32 + and Au Nanoparticles-Doped β-Cyclodextrin-Pb (II) Metal-Organic Framework. ACS Appl Mater Interfaces 8: 10121–10127. https://dx.doi.org/10.1021/acsami.5b11991
19. He T, Zhou T, Wan Y, Tan T (2020). A simple strategy based on deep eutectic solvent for determination of aflatoxins in rice samples. Food Anal Methods 13: 542–550. https://dx.doi.org/10.1007/s12161-019-01665-7
20. Myndrul V, Coy E, Bechelany M, Iatsunskyi I (2021) Photoluminescence label-free immunosensor for the detection of Aflatoxin B1 using polyacrylonitrile/zinc oxide nanofibers. Mater Sci Eng C Mater Biol Appl 118: 111401. https://dx.doi.org/10.1016/j.msec.2020.111401
21. Oliveira RC, Cortes-Eslava J, Gomez-Arroyo S, Carvajal-Moreno M (2021) Mutagenicity assessment of aflatoxin B1 exposed to essential oils. Lwt 140: 110622. https://dx.doi.org/10.1016/j.lwt.2020.110622
22. Prabhu SM, Kancharla S, Park CM, Sasaki K (2019) Synthesis of modulator- driven highly stable zirconium- fumarate frameworks and mechanistic investigations of their arsenite and arsenate adsorption from aqueous solutions plus Phi. CrystEngComm 21: 2320–2332. https://dx.doi.org/10.1039/c8ce01424h
23. Rushing BR, Selim MI (2019) Aflatoxin B1: A review on metabolism, toxicity, occurrence in food, occupational exposure, and detoxification methods. Food Chem Toxicol 124: 81–100. https://dx.doi.org/10.1016/j.fct.2018.11.047
24. Shen H, Shi H, Yang Y, Song J, Ding C, Yu S (2022) Highly efficient synergistic biocatalysis driven by stably loaded enzymes within hierarchically porous iron/cobalt metal-organic framework via biomimetic mineralization. J Mater Chem B 10: 1553–1560. https://dx.doi.org/10.1039/d1tb02596a

25. Wang S, Wang Z, Zhang L, Xu Y, Xiong J, et al (2022) Adsorption and convenient ELISA detection of sulfamethazine in milk based on MOFs pretreatment. Food Chem 374: 131712. https://dx.doi.org/10.1016/j.foodchem.2021.131712
26. Xu Z, Long L-L, Chen Y-Q, Chen M-L, Cheng Y-H (2021a) A nanozyme-linked immunosorbent assay based on metal-organic frameworks (MOFs) for sensitive detection of aflatoxin B1. Food Chem 338: 128039. https://dx.doi.org/10.1016/j.foodchem.2020.128039
27. Xu Z, Li L, Li K, Chen M-L, Tu J, et al (2021b) Peroxidase-mimetic activity of a nanozyme with uniformly dispersed Fe_3O_4 NPs supported by mesoporous graphitized carbon for determination of glucose. Mikrochim Acta 188: 1–10. https://dx.doi.org/10.1007/s00604-021-05035-1
28. Xu Z, Zhang L-w, Long L-l, Zhu S-h, Chen M-l, et al (2020) Metal Organic Frame-Upconverting Nanoparticle Assemblies for the FRET Based Sensor Detection of Bisphenol A in High-Salt Foods. Front Bioeng Biotechnol 8: 626269. https://dx.doi.org/10.3389/fbioe.2020.626269
29. You M, Peng P, Xue Z, Tong H, He W, et al (2021) A fast and ultrasensitive ELISA based on rolling circle amplification. Analyst 146: 2871–2877. https://dx.doi.org/10.1039/d1an00355k
30. Yu FY, Gribas AV, Vdovenko MM, Sakharov IY (2013) Development of ultrasensitive direct chemiluminescent enzyme immunoassay for determination of aflatoxin B1 in food products. Talanta 107: 25–29. https://dx.doi.org/10.1016/j.talanta.2012.12.047
31. Yu Z, Tang Y, Cai G, Ren R, Tang D (2019) Paper Electrode-Based Flexible Pressure Sensor for Point-of-Care Immunoassay with Digital Multimeter. Anal Chem 91: 1222–1226. https://dx.doi.org/10.1021/acs.analchem.8b04635
32. Zaib Q, Adeyemi I, Warsinger DM, AlNashef IM (2020) Deep Eutectic Solvent Assisted Dispersion of Carbon Nanotubes in Water. Front. Chem 8: 808. https://dx.doi.org/10.3389/fchem.2020.00808
33. Zavala-Franco A, Arambula-Villa G, Ramirez-Noguera P, Maria Salazar A, Sordo M, et al (2020) Aflatoxin detoxification in tortillas using an infrared radiation thermo-alkaline process: Cytotoxic and genotoxic evaluation. Food Control 112: 107084. https://dx.doi.org/10.1016/j.foodcont.2019.107084
34. Zhang J, Xu X, Qiang Y (2020) Ultrasensitive electrochemical aptasensor for ochratoxin A detection using AgPt bimetallic nanoparticles decorated iron-porphyrinic metal-organic framework for signal amplification. Sens. Actuators B Chem 312: 127964. https://dx.doi.org/10.1016/j.snb.2020.127964
35. Zhang Y, Li M, Cui Y, Hong X, Du D (2018) Using of Tyramine Signal Amplification to Improve the Sensitivity of ELISA for Aflatoxin B-1 in Edible Oil Samples. Food Analytical Methods 11: 2553–2560. https://dx.doi.org/10.1007/s12161-018-1235-9
36. Zhao Y, Yang Y, Luo Y, Yang X, Li M, Song Q (2015) Double Detection of Mycotoxins Based on SERS Labels Embedded Ag@Au Core-Shell Nanoparticles. ACS Appl Mater Interfaces 7: 21780–21786. https://dx.doi.org/10.1021/acsami.5b07804
37. Wang M, Duan M, Yu F, Fu X, Meng S (2021). Development of aflatoxin b1 aptamer sensor based on iron porphyrin organic porous material. Food Anal Methods 14: 1–8. https://dx.doi.org/10.1007/s12161-020-01877-2

Figures

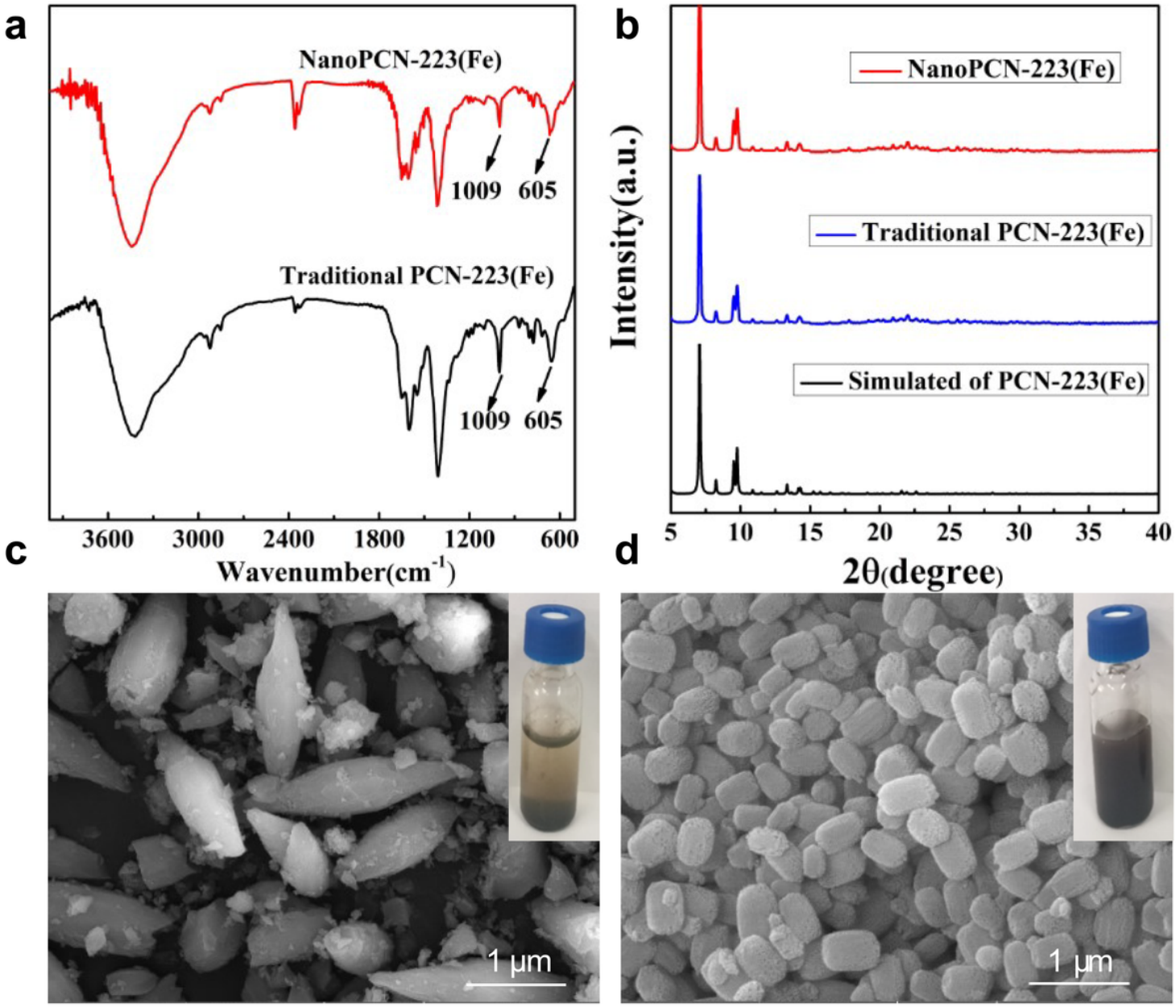

Figure 1

Characterize the synthesis of NanoPCN-223(Fe): (a) FTIR spectra and XRD patterns (b) of NanoPCN-223(Fe) and traditional PCN-223(Fe). (c) Scanning electron microscopy image of traditional PCN-223(Fe) and NanoPCN-223(Fe) (c and d) The photographs inserted in panels c and d indicate the dispersion of an aqueous solution of traditional PCN-223(Fe) (c) and NanoPCN-223(Fe) (d) after 24 h.

Figure 2

Confirm the enhanced dispersion of NanoPCN-223(Fe): (a-c) DLS results of (a) NanoPCN-223(Fe), (b) traditional PCN-223(Fe) and (c) MIL-88. (d) Zeta-potential of traditional PCN-223(Fe), NanoPCN-223(Fe), and MIL-88.

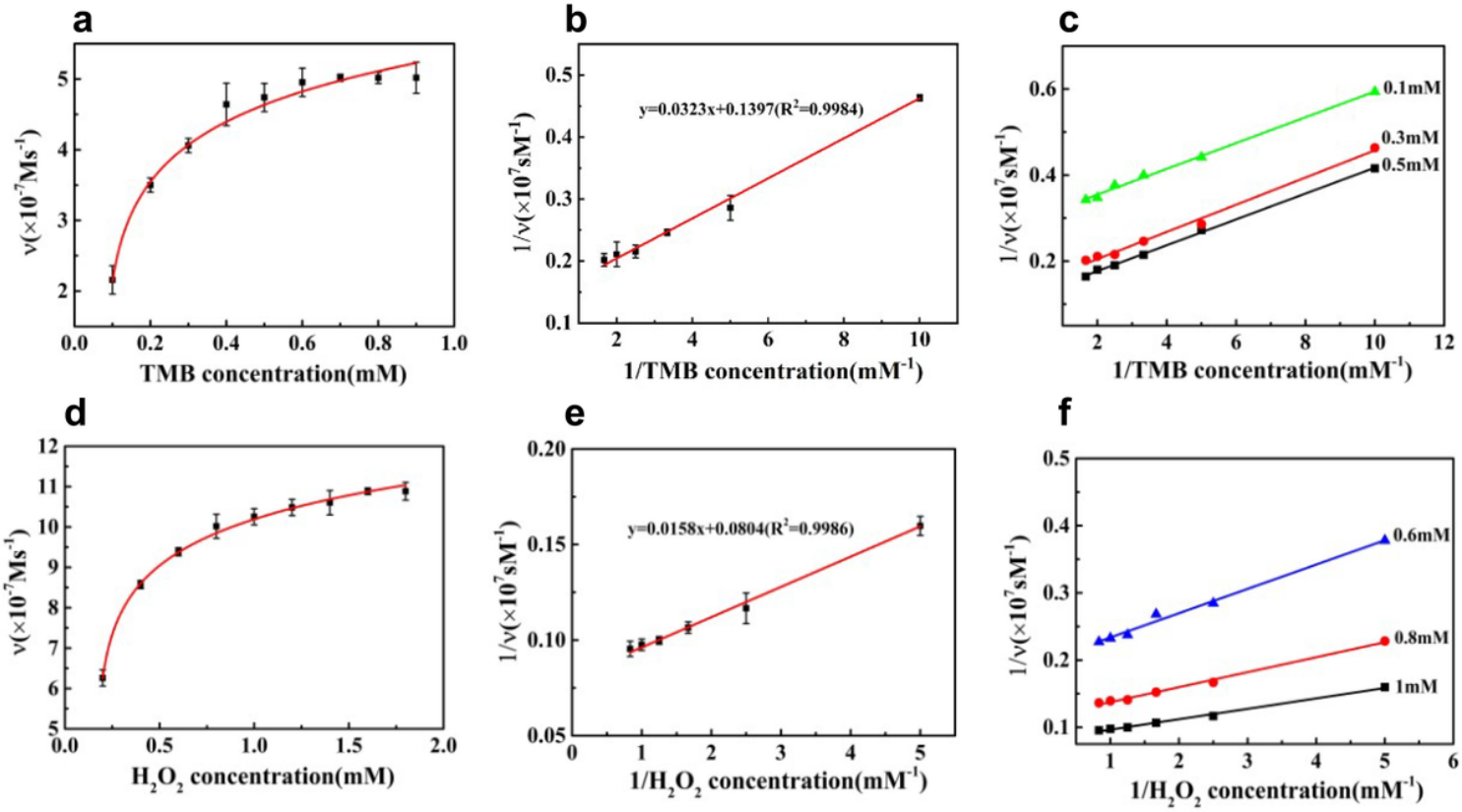

Figure 3

Kinetic assays of NanoPCN-223(Fe) as catalysts for TMB oxidation. (a-c) Kinetic assays of TMB. (A) Plot of v against TMB concentration, with H_2O_2 concentration fixed at 0.3 mM. (b) Double-reciprocal plot generated from (a). (c) Double-reciprocal plots at different H_2O_2 concentrations. (d-f) Kinetic assays of H2O2. (d) Plot of v against H_2O_2 concentration, with TMB concentration fixed at 1 mM. (e) Double-reciprocal plot generated from (d). (f) Double-reciprocal plots at different TMB concentrations.

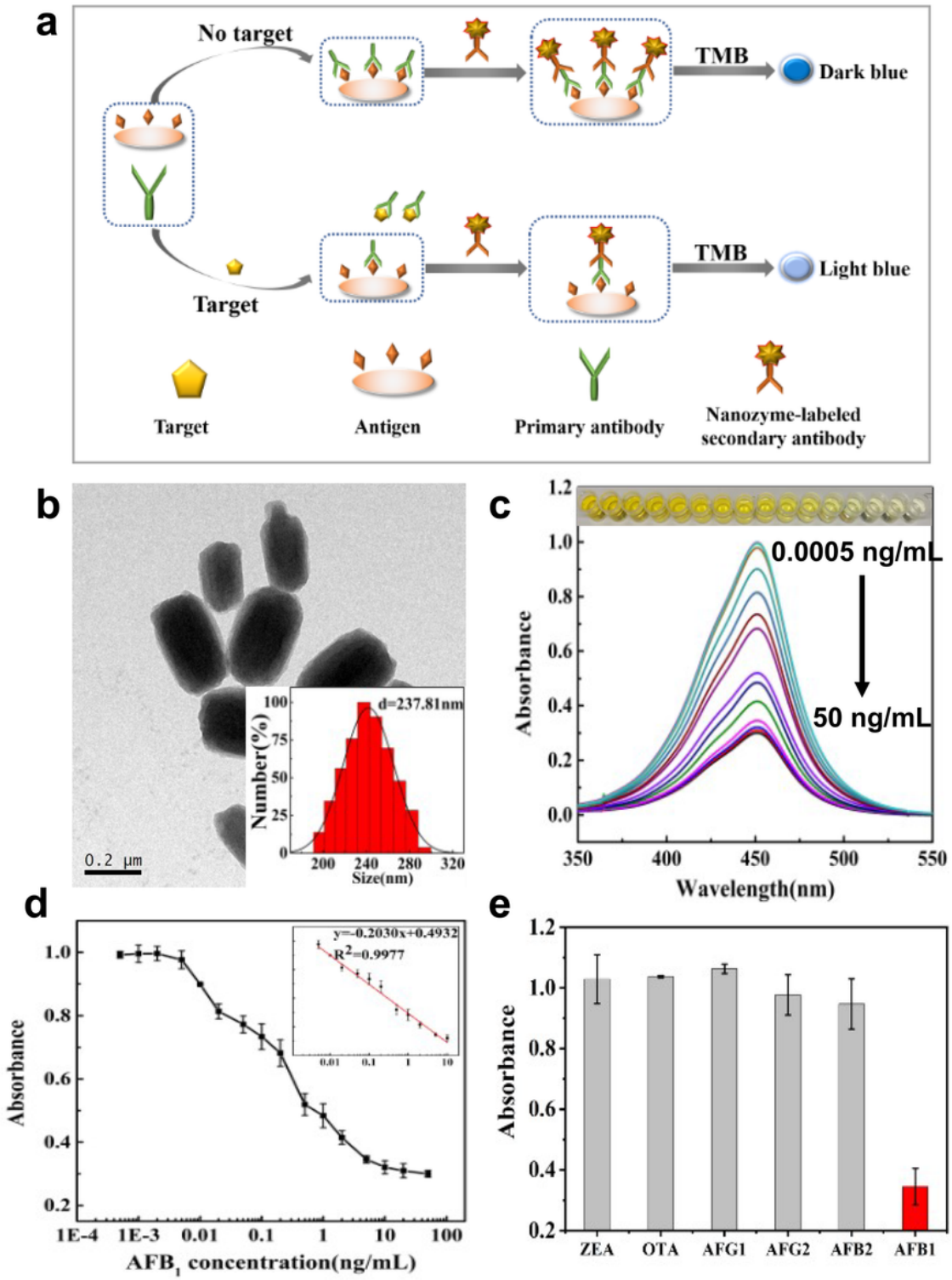

Figure 4

The performance of Ed-MOFLISA for the detection of AFB1: (a) Schematic illustration of Ed-MOFLISA for the detection of AFB1. (b) Transmission electron microscopy and dynamic light scattering images of NanoPCN-223(Fe)@Ab2. (c) Absorption spectra of various AFB1 concentrations within the range of the standard curve. (d) Response curves of AFB1. Error bars represent the standard deviation for three

measurements. The insert shows the linear relationship between absorbance and AFB1. (e) Detection specificity of AFB1 (5 ng/mL) and ZEA, OTA, AFG1, AFG2, and AFB2 (each 25 ng/mL).

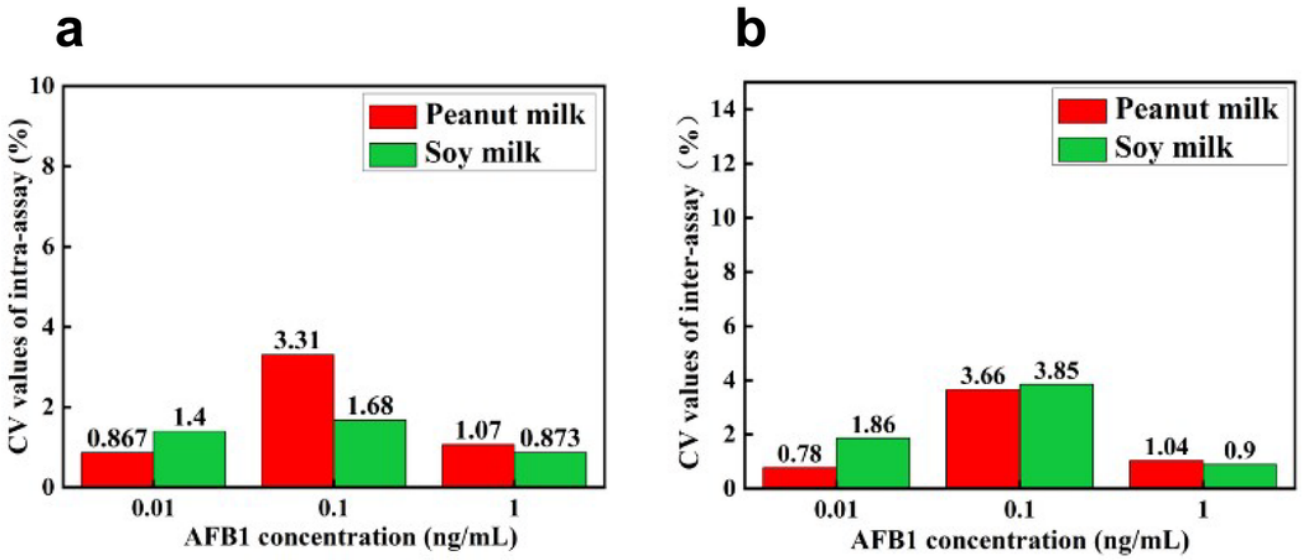

Figure 5

Reproducibility of Ed-MOFLISA: (a)The CV values of intra-assay; (b) The CV values of inter-assay

Supplementary Files

This is a list of supplementary files associated with this preprint. Click to download.

- SupportingInformation.docx